PHILOSOPHICAL TRANSACTIONS OF THE ROYAL SOCIETY A MATHEMATICAL, PHYSICAL & ENGINEERING SCIENCES

Intracontinental Seismicity, Strength of Crustal Units, and the Seismic Signature of Fault Zones

R. Meissner and T. Wever

Phil. Trans. R. Soc. Lond. A 1986 **317**, 45-61
doi: 10.1098/rsta.1986.0024

Phil. Trans. R. Soc. Lond. A **317**, 45–61 (1986) [45]
Printed in Great Britain

Intracontinental seismicity, strength of crustal units, and the seismic signature of fault zones

By R. Meissner and T. Wever
Institut für Geophysik, Neue Universität, Olshausenstrasse 40–60, 2300 *Kiel, F.R.G.*

The distribution of intracontinental seismicity in the upper crust is compared with theoretically obtained strength–depth curves based on recent laboratory data from cold and brittle frictional sliding, as well as from high-temperature creep data. The lower crust is seen as a channel of enhanced ductility like jelly in a sandwich. This rheological picture is compatible with the formation of mylonites in the lower crust and the appearance of cataclasites in the rigid upper crust. Sub-horizontal zones of detachment prefer the upper part of the ductile lower crust in the continents resulting in the formation of crustal nappes during compressional phases. The most active fault zones seem to exhibit reduced values of brittle, elastic and inelastic parameters.

1. Introduction

Epicentres of intracontinental earthquakes are concentrated on lineaments. Stresses based on focal plane solutions mostly coincide with the stress pattern obtained from the observations along geologically young structures, such as rifts and grabens with normal faulting, or overthrusts and strike-slip faults with their seismic equivalent (Zoback & Zoback 1981). Another observation, not so widely known, is the restriction of hypocentres to the upper crust. The shallow depth of seismicity has been related to the onset of creep phenomena in the middle crust. A possible correlation between the peak seismicity or the deepest seismic events with the temperature or viscosity régime of crustal units has been suggested (Meissner & Strehlau 1982, 1985; Sibson 1982; Chen & Molnar 1983; Strehlau 1985). Some of these data will be reviewed in the first part of this paper, while new calculations on the ductility of the continental crust and their maximum stress levels will be the subject of the second part. In the third part, examples of reflecting fault zones will be shown and the reason for their reflectivity in the brittle, seismic upper crust and in the ductile, aseismic lower crust will be investigated. Finally, correlations between various crustal features will be discussed.

2. Intracontinental seismicity

As mentioned in the Introduction, earthquakes concentrate on certain lineaments, as seen in figure 1, showing a dynamically active part of the San Andreas Fault System (after Buffe *et al.* 1977). Seismicity is strongest along such intracontinental plate boundaries as the San Andreas or the North Anatolian Fault Zones. However, away from present plate boundaries inside the continents, the concentration of seismicity on fault zones is also apparent (Zoback & Healy 1984).

When old lineaments are reactivated under a new stress régime, the preference of stress release along them is indicative of their mechanical weakness. The new stress pattern might be similar to an older one, as for the Alpine orogeny and the Devonian–Carboniferous Variscan tectonics

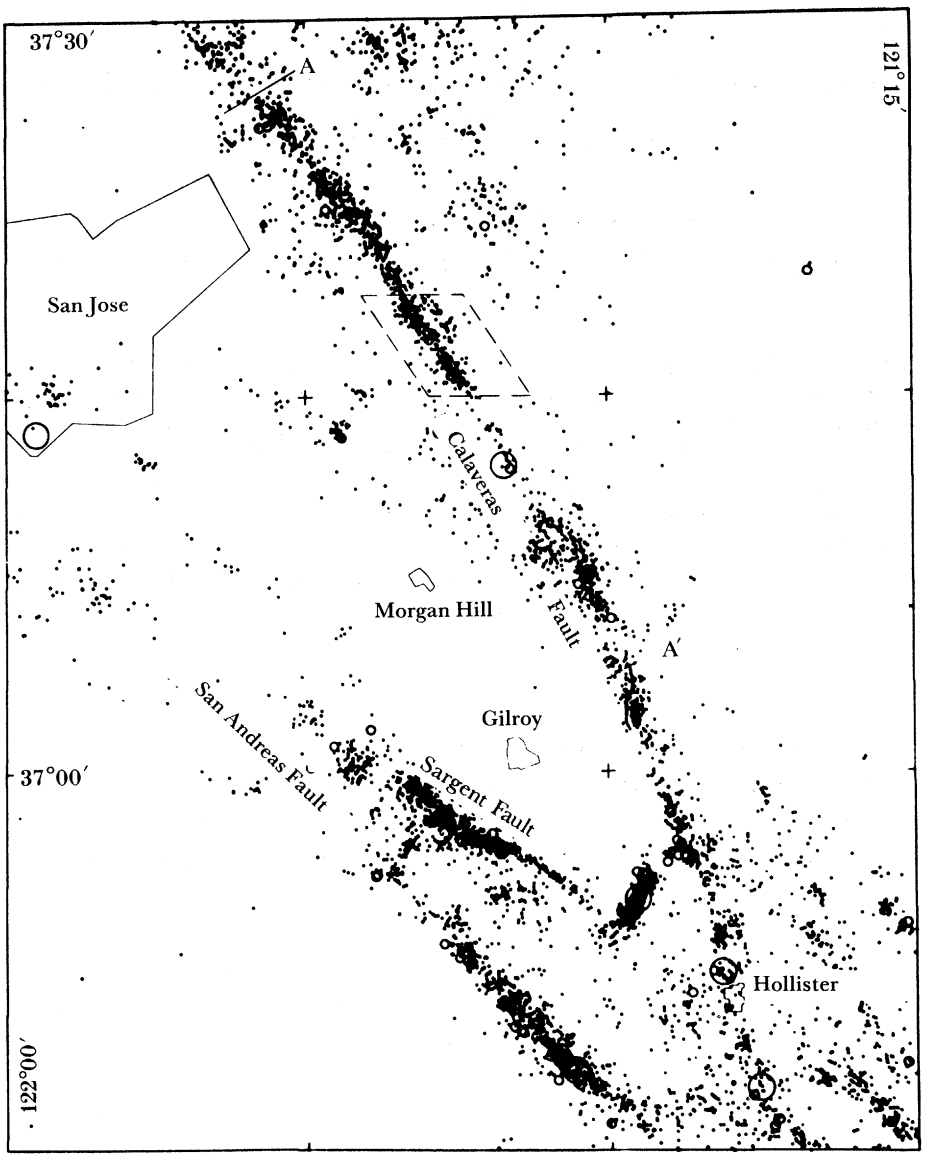

FIGURE 1. Distribution of seismicity along the southern part of the San Andreas Fault System (after Buffe *et al.* 1977). Seismicity is concentrated on short (Sargent Fault) and long Calaveras Fault) lineaments. ○, events with magnitude < 3.0; ○, events with magnitude 3.0–4.5; ., events with magnitude 4.5–6.0. A–A′ is the situation of the profile in figure 2.

in Central Europe. It might be the reverse, as for the present extension of the Basin and Range Province compared with compression during the early Tertiary. Normal faulting might change to strike-slip movement as for parts of the Tornquist line and the eastern Rhinegraben Fault (Guterch 1977; Illies 1978). Apparently such lineaments survive the change of stress and strain release, at least in their observable near-surface areas.

While figure 1 is an example of measurements by a dense seismometer network in a seismically active area, figure 2 shows the restriction of seismicity to the upper 11 km along a section in the same area (Buffe *et al.* 1977). Such a distribution of earthquakes in the crust was the subject of several regional and global investigations, such as those of Meissner & Strehlau (1982, 1985)

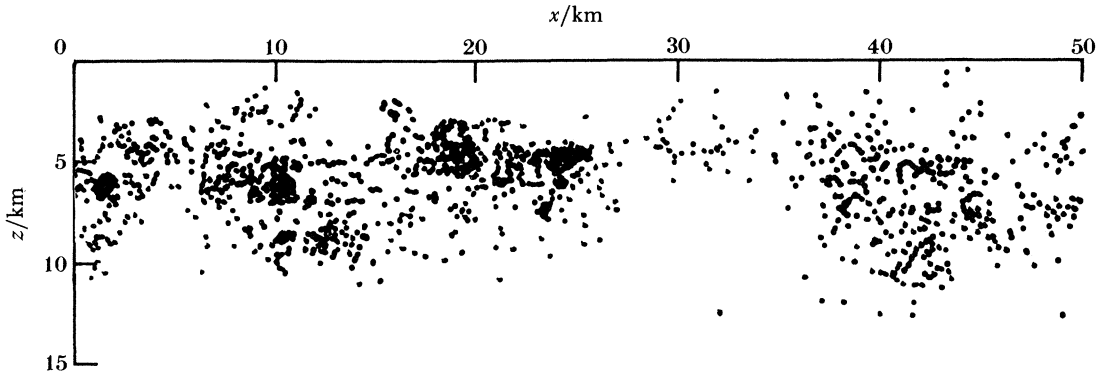

FIGURE 2. Distribution of seismicity in the upper 11 km along a part of the Calaveras Fault (after Buffe *et al.* 1977).

or Chen & Molnar (1983). The restriction of earthquakes to the upper crust is a truly general phenomenon in continental as well as in oceanic areas. Exceptions are found in areas where the cold lithosphere is forced to deeper levels in zones of recent subduction or suture, or in areas of exceptionally high strain rates, as in highly anomalous young areas like Tibet or volcanic areas like Hawaii. Chen & Molnar (1983) provide examples for some of these anomalous areas where, in addition to the earthquakes in the upper crust, some seismicity is seen in the uppermost mantle again, leaving the lower crust free of seismicity.

The peak of crustal seismicity and its maximum depth seem to be dependent on the temperature. Figure 3*a* shows normalized frequency–depth distributions of the Coso area in the western U.S.A. The whole geothermally anomalous area with rather high seismicity (more than 4000 events) shows a sharp peak at 5–6 km depth and a complete termination of seismicity at 16 km. The centre of the geothermally active area, with 'only' about 2000 events, shows quite a similar shape, but seismicity ends at 14 km. These figures were normalized with regard to the maximum number of earthquakes and a depth interval of 1 km (see Meissner & Strehlau 1982).

Figure 3*b* gives examples from the area of the Upper Rhinegraben, where seismicity (and the number of data points) is much lower than in the Coso area. Nevertheless, the seismicity inside the geothermally anomalous Rhinegraben Valley with a peak around 7 km and a termination at 16 km, is definitely shallower than that of the adjacent Black Forest (Schwarzwald), where heat flow is considerably lower, and also the peak and the termination of seismicity is at a much deeper level. Strehlau (1985) obtains a strong correlation between the heat flow and the maximum depth of earthquakes based on a huge collection of seismicity and geothermal data from continental areas.

There is no doubt that the restriction of seismicity to the upper crust and its correlation to the heat flow régime is the strongest argument for the ductility of the continental lower crust and for the strong influence of temperature. All seismicity–depth relations with at least 300 data points and a depth resolution of up to 1 km show a similar shape to figure 3*a*, although the peak and the maximum depths are deeper in low heat flow areas.

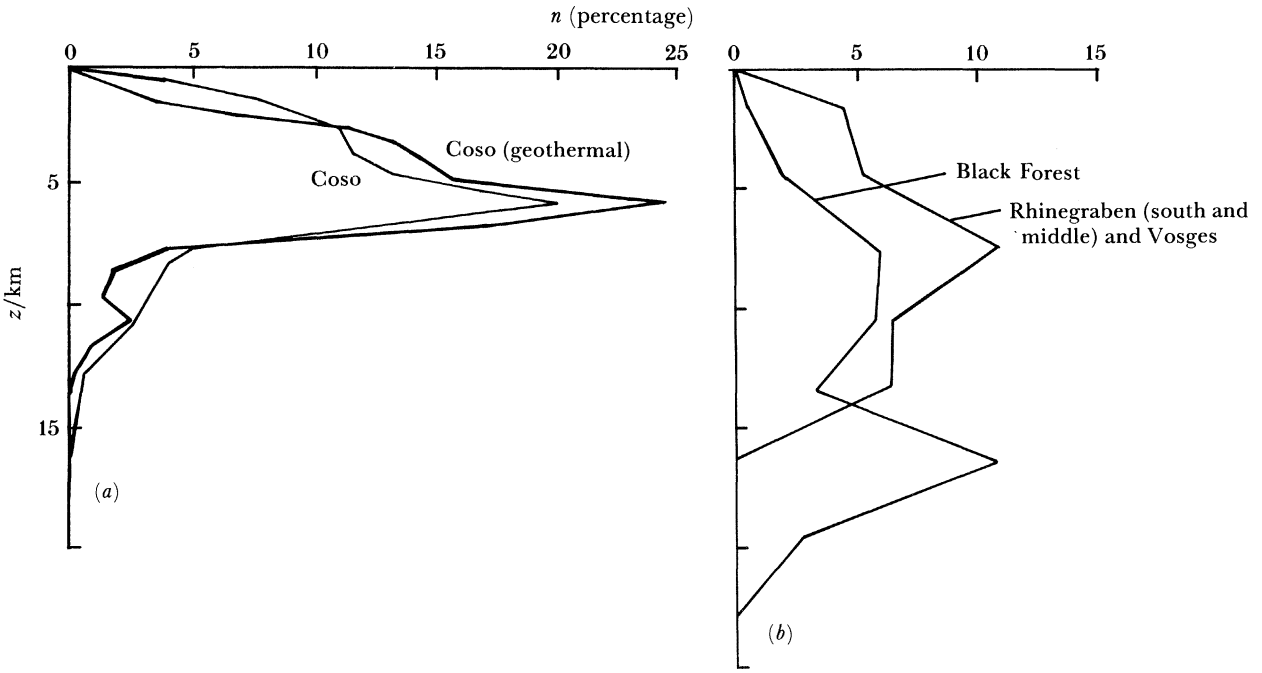

FIGURE 3. Seismicity–depth (n–z) functions (a) in the Coso area, western U.S.A. and (b) in the Rhinegraben area, western Europe.

TABLE 1. SEISMICITY–DEPTH DATA

	N	Δz/km	q_0/(mW m^{-2})
all Coso	4221	1	90
Coso geothermal	1950	1	$\geqslant 90$
Black Forest	98	3	< 70
Rhinegraben	83	3	> 90

N is the number of seismic events, z is the depth interval, and q_0 is the average heat-flow density.

3. THEORETICAL STRENGTH–DEPTH RELATIONS: MATCHING SEISMICITY–DEPTH CURVES

In the last decade, evidence has greatly increased to suggest that laboratory data of the frictional behaviour of rocks, i.e. relations between the ultimate frictional strength and normal stress, are good approximations to *in situ* observations of near-surface stresses in boreholes. (Brace 1972, 1979; Byerlee 1978; Zoback & Healy 1984). In particular, the work of Byerlee (1978) on fractured rocks provided the modern experimental verification of Coulomb's criterion from 1773 that

$$|\tau| = \sigma_0 + \mu^* \sigma_N, \tag{1}$$

where $|\tau|$ is the shear stress: here, the ultimate frictional strength; σ_N is the normal stress; $\sigma_0 = |\tau|$ for $\sigma_N = 0$ (inherent shear strength; cohesion); μ^* is the coefficient of internal friction.

Byerlee (1978) specifically showed that μ^* values of 0.6–0.85 fitted nearly all types of rocks, and only clay minerals like montmorillonite and vermiculite form some exceptions with μ^* around 0.2. In §3 the significance of μ^* values will be discussed again.

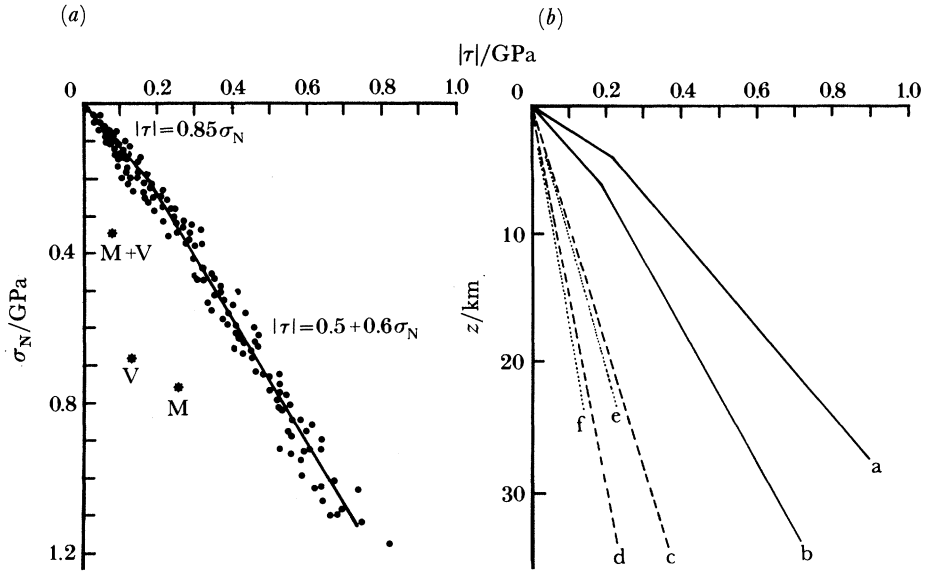

FIGURE 4. (*a*) Byerlee's (1978) data from frictional sliding experiments on pre-cut samples of various rocks; m, montmorillonite; v, vermiculite. (*b*) Calculation of maximum stresses (i.e. frictional strength) from Byerlee's (1978) data: a, compression (σ_1 horizontal), no pore pressure: b, compression (σ_1 horizontal), hydrostatic pore pressure; c, extension (σ_3 horizontal), no pore pressure; d, extension (σ_3 horizontal), hydrostatic pore pressure; e, compression (σ_1 horizontal), for m+v (no pore pressure); f, compression (σ_1 horizontal), m+v (hydrostatic pore pressure).

Figure 4*a* shows Byerlee's data in a τ–σ_N diagram, using

$$|\tau| = 0.85\sigma_N \tag{2}$$

for the uppermost part, and

$$|\tau| = 0.5+0.6\sigma_N \tag{3}$$

for the lower (main) part of the curve. An introduction of these values into the two-dimensional stress equation (Jaeger 1969) provides different relations for compression (σ_1 horizontal) or extension (σ_1 vertical), with σ_1 equivalent to the maximum principal stress (Sibson 1974). Relating σ_1 and σ_3 (the minimum principal stress) to depth by

$$\sigma_3 = gz(\rho-\rho_{H_2O}) \tag{4}$$

for compression and

$$\sigma_1 = gz(\rho-\rho_{H_2O}) \tag{5}$$

for extension, the solid lines in figure 4*b* are obtained; g is the surface gravity, z is the depth, ρ is the density under lithostatic pressure and ρ_{H_2O} is the density of hydrostatically loaded pore fluid. Hence figure 4*b* is a formal 'cold' application of Byerlee's relation to the Earth's crust (Meissner & Strehlau 1982). 'Cold' means that no influence of the increasing temperature with depth is involved in this relation.

Today, a wide range of experiments with high-temperature creep data is available even for crustal rocks and minerals (Kirby 1983). From these data the activation energy for creep processes and other parameters can be taken and introduced into the general creep equation (Weertman 1970; Weertman & Weertman 1975).

$$\dot{\epsilon} = C_n \tau^n \exp\,[-(E_c^*/RT)], \tag{6}$$

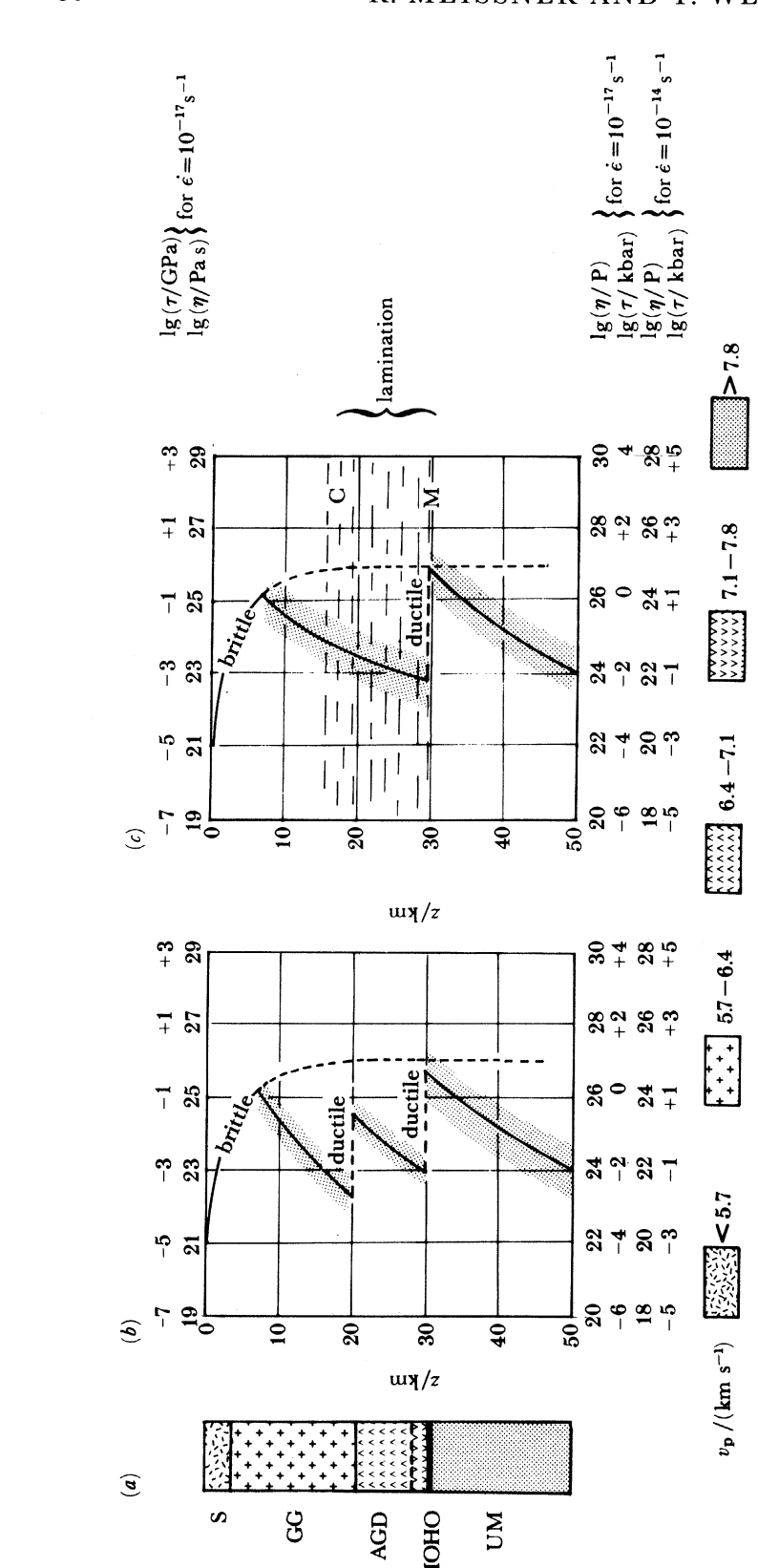

FIGURE 5. (*a*) Simplified velocity–depth column for Variscan areas (Meissner 1985). (*b*) Strength–depth and viscosity–depth curves for the crustal model of (after Meissner & Strehlau 1985). (*c*) Smoothed strength–depth (viscosity–depth) curves based on a gradational transition of velocities and rock types; lamination represents the zone of strongly increased density of seismic reflectors; S, sediments; GG, granitic–gneissic; AGD, amphibolites, granulites, dioritic rocks; UM, ultramafic rocks of the upper mantle. Numbers are seismic velocities in kilometres per second; η, viscosity; τ, shear stress; v_p, seismic velocity of compressional waves; C, Courad discontinuity; M, Mohorovičić discontinuity. For details see text. Dotted area around solid line indicates the η and τ ranges obtained from four rock types with slightly different creep parameters in each unit; upper mantle creep data from Kirby (1983).

where $\dot{\epsilon}$ is the creep rate, E_c^* is the 'effective' activation energy, C_n is a constant, R is the gas constant, τ is the differential stress, T, the temperature in kelvins and n is an exponent ($n = 1 \ldots 4$). Equation (6) can be solved for τ or for $\eta = \tau/\dot{\epsilon}$, resulting in the two similar equations:

$$\ln \tau = (1/n)\,(E_c^*/RT + \ln \dot{\epsilon} - \ln C_n) \tag{7}$$

and

$$\ln \eta = (1/n)\,[E_c^*/RT + (1-n)\ln \dot{\epsilon} - \ln C_n]. \tag{8}$$

Equation (7) gives the stress level which accompanies the creep process, while (8) gives the effective viscosity for steady-state creep. From (7) and (8), there is a proportionality between $\ln\tau$ and $\ln\eta$. The strong dependence of $\ln\eta$ and $\ln\tau$ on the temperature, T, suggests that at a certain depth, $z(T)$, stresses calculated by Byerlee's relation (figure 4*b*) will not be reached because creep processes with their lower stresses will begin. Depending on the creep rate $\dot{\epsilon}$, the specific rock type with its individual E_c^* (including the influence of water), and the other creep parameters n and C_n, the depth where creep starts to dominate may vary. But because of the non-logarithmic influence of T, the influence of temperature is the strongest one.

Figure 5*a* shows a simplified velocity column, typical for Variscan areas (Meissner 1985). For each of the three major units, upper crust (without sediments), lower crust, and upper mantle, four rocks and minerals, compatible with the velocity data, were selected from Kirby's (1983) list as follows. Wet granite, dry granite (two), and wet quartzite for the upper crust; quartz diorite, albite, dry quartz and dry basalt for the lower crust; and olivines, peridotites and dunite for the uppermost mantle. By using a typical Variscan surface heat-flow density of 65 mW m^{-2} and conventional temperature–depth curves $T(z)$ or $z(T)$ from Strehlau (1985), $\ln\tau(z)$ and $\ln\eta(z)$ curves are easily obtained. Table 2 shows a list of rock types and related

TABLE 2. PROPERTIES OF ROCK TYPES

rock type	$E_c^*/(\mathrm{KJ\ mol^{-1}})$	n	$\lg C_n/(\mathrm{GPa^{-n}\ s^{-1}})$	symbols (figures 5, 6)
dry granite	106	2.9	0.2	GG
dry granite	139	3.4	1.6	(upper crust)
wet granite	137	1.9	2.0	
wet quartzite	160	2.4	3.2	
wet quartzite	134	2.6	3.0	
wet quartzite	167	1.8	3.7	
quartz diorite	219	2.4	4.3	AGD–MG
diabase	260	3.4	6.5	(lower crust)
albite rock	234	3.9	6.1	
dry quartzite	184	2.8	2.0	
olivine	498	4.5	16.1	upper mantle
dunite	444	3.4	14.0	

Parameters for equations (6), (7), (8) used for the calculation of the viscosity–depth curves of figures 5, 6. For symbols see figures 5, 6. Data from Kirby (1983).

parameters which are used for the calculation of the curves in figures 5*b*, *c* and 6*b*, *c*. The curves represent averages of six (upper crust), four (lower crust) and two (upper mantle) individual viscosity–depth curves. Figure 5*b* shows the average η and τ data for creep rates of $\dot{\epsilon} = 10^{-17}$ s^{-1} and 10^{-14} S^{-1}. Note that Byerlee's 'brittle' curve is transformed to the logarithmic scale. The dotted area around the solid line in the middle and lower part of the figure shows the η and

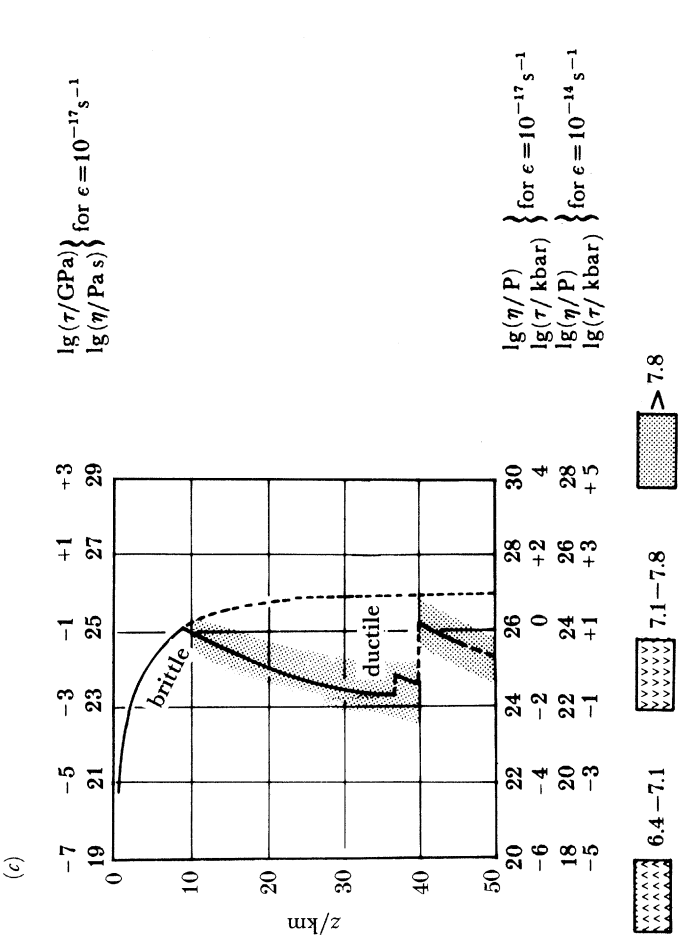

FIGURE 6. (*a*), (*b*), (*c*) Same relations as those of figure 5. MG, mafic granulites, serpentinites.

τ ranges from the mentioned rock types, assuming that at the Conrad level, at 20 km, rocks from the upper crust change to lower-crustal rock types and again to mantle rocks at about 30 km, i.e. at the Moho level. A more gradational change of rocks from upper to lower crust, compatible with a more transitional velocity–depth function is depicted in figure 5*c*. One may deduce from these data that the lower crust with its missing seismicity is certainly a zone of low viscosity. It might be added that an increased water content in the lower crust or a viscosity-dependent creep rate would still enhance this effect.

Figure 6*a*, *b*, *c* shows the equivalent diagrams for a typical shield area with smaller surface heat flow (55 mW m^{-1}) and deeper Moho. Viscosities and creep stresses are about one order of magnitude higher, mostly an effect of temperature. In particular, old shields are less ductile and less deformable than younger crustal units. It should be stressed that the viscosity–depth values of figures 5 and 6 are based on experimental data of rock types which do not necessarily represent the mylonite facies that are supposed to dominate in the lower part of the crust. Once increased strain concentrates on certain lineaments, strain rate, $\dot{\epsilon}$, might increase by several orders of magnitude, also enhancing τ and η in (7) and (8). For the brittle part of the crust, Byerlee's law (1978) is supposed to dominate. Microcracks in the upper crust, equivalent to the pre-broken rocks in the experiments, might be considered as representative of the *in situ* condition. But a coalescence of microcracks into a large rupture and the formation of a large fault zone also changes the stress conditions and especially the σ_0 values of (1) (see also §4). In conclusion, both the brittle and the ductile relations in figures 5 and 6 seem to represent crustal structures which are not (or not yet) affected by *large* fault zones.

There is a good correlation between the seismicity–depth curve and the combined brittle–ductile strength curve in the upper part of the crust. For a wet upper crust both peaks agree and seem to be dependent on the temperature, as shown in the two examples of figure 7. The distribution of seismicity in the crust is definitely a function mainly of the temperature (or viscosity).

Exceptions are possible, even away from plate boundaries in tectonically very active areas, along *narrow* faults and volcanic pipes where $\dot{\epsilon}$ and τ might increase considerably; τ might cross

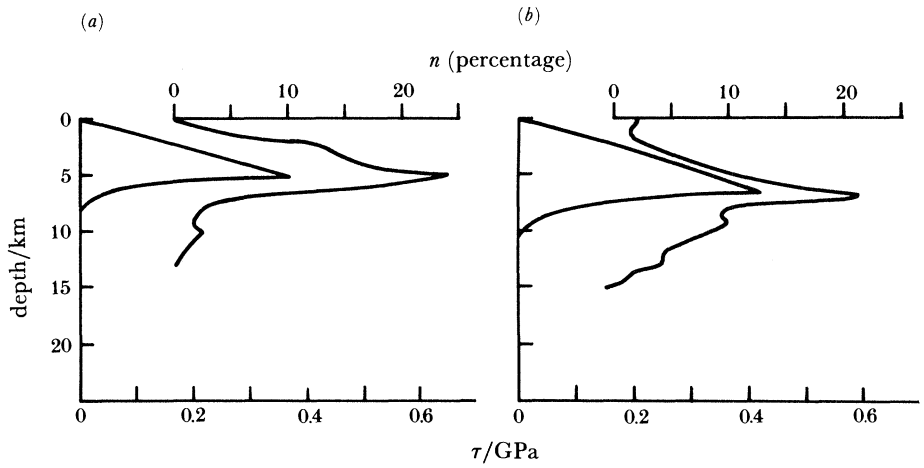

FIGURE 7. Comparison of seismicity–depth (n–z) with strength–depth (τ–z) curves. (*a*) Coso, high heat flow area, $q = 90$ mW m^{-2}; (*b*) Greece, medium heat flow area, $q = 70$ mW m^{-2}. Combined τ–z curves are for brittle behaviour with hydrostatic pore pressure (upper part) and for wet rocks and ductile behaviour (lower part).

the brittle curve again and give rise to a seismic energy release, preferably in the uppermost mantle where the curves nearly meet in our diagrams, in accordance with the observations of Chen & Molnar (1983).

4. The seismic picture of fault zones

Fault-related rocks are known to be the result of an interplay between strain and recovery (Wise *et al.* 1984). In the upper, brittle part of the crust there are the cataclasites which have undergone rapid strain at rather low temperatures. They may consist of breccia or microbreccia, indicating a coseismic energy release, or of 'gouge' or 'rock flour' indicating energy release by (episodic) creep events, even in the uppermost crust. Hence, the upper crust is the place of seismic *and* aseismic energy release. Typical fault-related rocks of the lower crust are the mylonites, marked by relatively high strain rates with generally appreciable recovery rates. They behave completely aseismically, unless they are transferred to the brittle and cold upper crust.

In contrast to the cataclasites, mylonites have at least a microscopic foliation. In the lower crust, one may also call them 'ductile' fault material compared to the 'brittle' faults of the upper crust. The San Andreas Fault seems to consist of 5 km of incohesive gouge, followed by cohesive microbreccias down to 10–15 km underlain by 'quasi-plastic' mylonites (Sibson 1977), a model which is compatible with the viscosity models of §3. The fault zones of the upper crust with their gouge material have definitely lower seismic velocities than their surroundings, as found by laboratory and *in situ* measurements (Wang 1984). More controversial data are reported about mylonites; they may have lower or higher velocities than the host rocks, depending apparently on the degree of strain (with strong weakening) or recovery (with a strengthening of the rock matrix) (Jones & Nur 1982, 1984; Fountain *et al.* 1984).

In spite of the different mechanism and composition of fault zones in the upper and lower crust, they seem to be seismically reflective in the whole crust. It may be noted that reflection seismics is the only geophysical method able to detect lineaments with such a small width. In figure 8 a summary of seismically mapped fault zones is presented, 8*a–d* showing extensional structures, and 8*e–h* showing compressional features.

Steep-angle normal faults associated with half grabens are depicted in figures 8*a*, *b*, the former showing a post-Variscan and the latter a Tertiary rift feature. Low-angle extensional faults are also possible (figures 8*c*, *d*). Their sub-horizontal zone of detachment appears to favour the depth of the brittle–ductile transition. Often their listric shape ends in a sub-horizontal fault, behaviour that directly indicates the transition to a ductile behaviour at depth.

Compressional thrust faults have generally shallow dips and often sub-horizontal parts, as shown in figures 8*e–h*. There is a relation between the coefficient of friction (μ^*) to the angle (α) between σ_1 and the trace of the fault (Jaeger 1969):

$$\mu^* = ctg(2\alpha). \tag{9}$$

This relation, developed for brittle (not ductile) behaviour, may formally result in angles between $\alpha = 0$ (for $\mu^* \to \infty$) and $\alpha = 45°$ (for $\mu^* \to 0$).

In practice however, values of α between 20° and 40° have to be assumed as shown in table 3. This means that shallow-field angle thrust faults are possible in a brittle medium. Shallow-angle extensional faults, however, with $\alpha > 45°$, are strictly forbidden in a brittle medium. But such

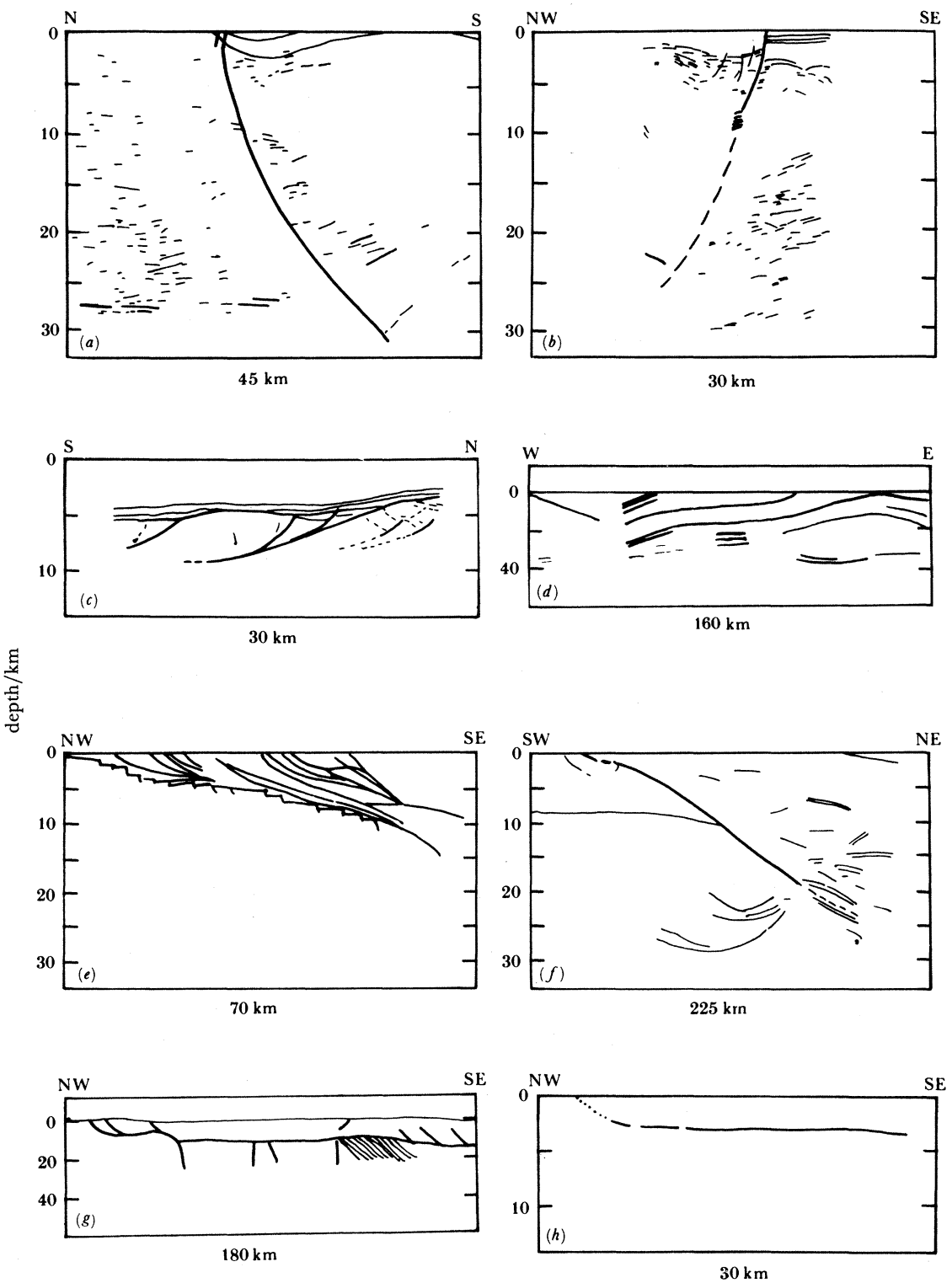

FIGURE 8. Seismic signature of fault zones in reflection seismogram sections (line drawings). (*a*)–(*d*) Show extension régimes: (*a*) Hunstrück boundary fault, SW Germany; (*b*) Rio Grande Rift, COCORP; (*c*) Gulf of Biscay, France; (*d*) Basin Range Province, COCORP. (*e*)–(*h*) Show compressional features: (*e*) Northern Appalachians near Quebec; (*f*) Wind River Mountains, COCORP; (*g*) Southern Appalachians, COCORP; (*h*) Aachen–Hohes Venn area, Germany. (After various authors, summarized in Meissner (1985)).

PHILOSOPHICAL TRANSACTIONS OF THE ROYAL SOCIETY A MATHEMATICAL, PHYSICAL & ENGINEERING SCIENCES

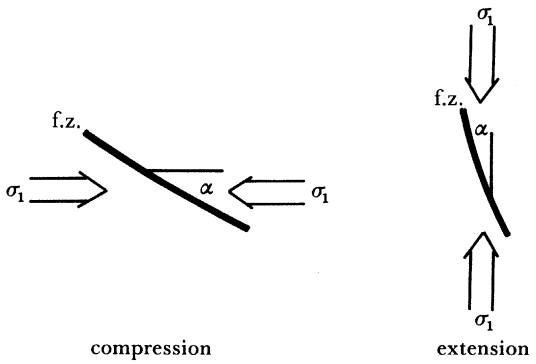

FIGURE 9. Shows relation of table 2. F.z. represents fault zone.

TABLE 3. VALUES OF μ^* AND α

μ^*	α	remarks
0	45.0	clays, loess (?)
0.18	39.9	clay minerals (montmorillonit, vermiculite)
0.3	36.7	sands
0.4	34.1	big faults in Nature
0.6	29.5	pre-cut rocks + borehole data
0.85	24.8	pre-cut rocks at $p \approx 0$ + borehole data
1	22.5	geologic structure + borehole data
∞	0	

The coefficient of friction related to the angle between the trace of the fault and the maximum principal stress, σ_1, according to equation (9). See figure 9.

faults do occur in nature, which means that they are outside the brittle régime. Hence the listric shape of extensional (normal) faults may indicate the transition zone from the brittle to the ductile régime.

Reflection seismics usually provides the general shape of fault zones. Shallow-angle fault zones can be much better observed than steep-angle fault zones because of the generally short distances between shots and receivers.

Sometimes, a careful analysis of the seismic signal gives additional information. The reflection polarity reflects the impedance, ρV, inside the fault zones, i.e. in general the velocity V. Negative polarity means that the interior of the fault has lower seismic velocities than its host rocks, as shown for the example of the Aachen–Hohes Venn overthrust, where 70% of all values show a clear negative polarity. Figure 10 gives detail of figure 8*h* (Meissner *et al.* (1981)). As mentioned, cataclasites in the brittle part of the crust generally have lower velocities. An example for reflections from a steep-dipping near-surface fault is provided by figure 11 (Rabbel 1985). Here, a reflected refraction is seen only in the vertically and horizontally polarized shear waves (s.v. and s.h.) not in compressional (p) waves. Apparently, the shear modulus μ shows a big contrast between cataclasite and host rock, or a favourable relation of fault widths to wavelength results in a constructive interference for shear waves only. As mentioned before, steep-dipping fault zones at great depth are hard to observe because of problems with the shot-receiver geometry. It was a lucky coincidence during a survey across the Hunsrück boundary fault that seismic signals with an apparent velocity of nearly ∞ were observed by some nearby refraction stations. The same high apparent velocity (which means vertical

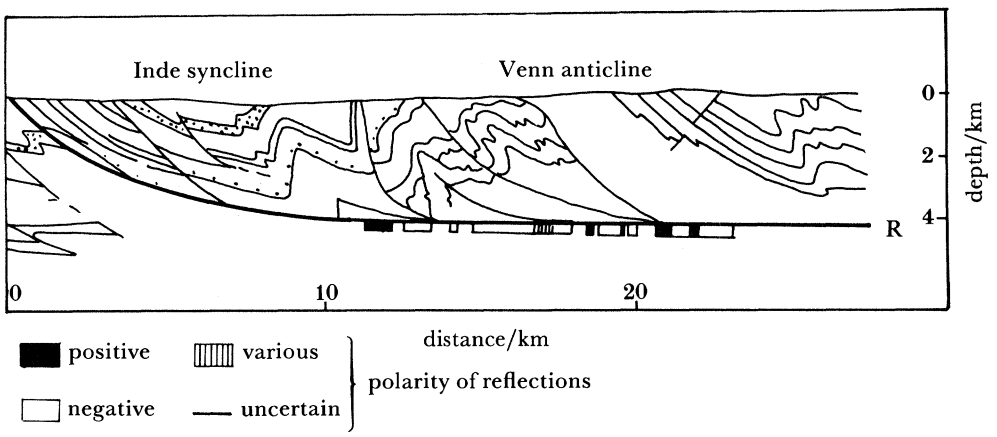

FIGURE 10. Geologic cross section of the Aachen overthrust with seismic reflector (R) and polarity of reflections as determined along R in areas of strong signal:noise ratios; see also figure 8*h*.

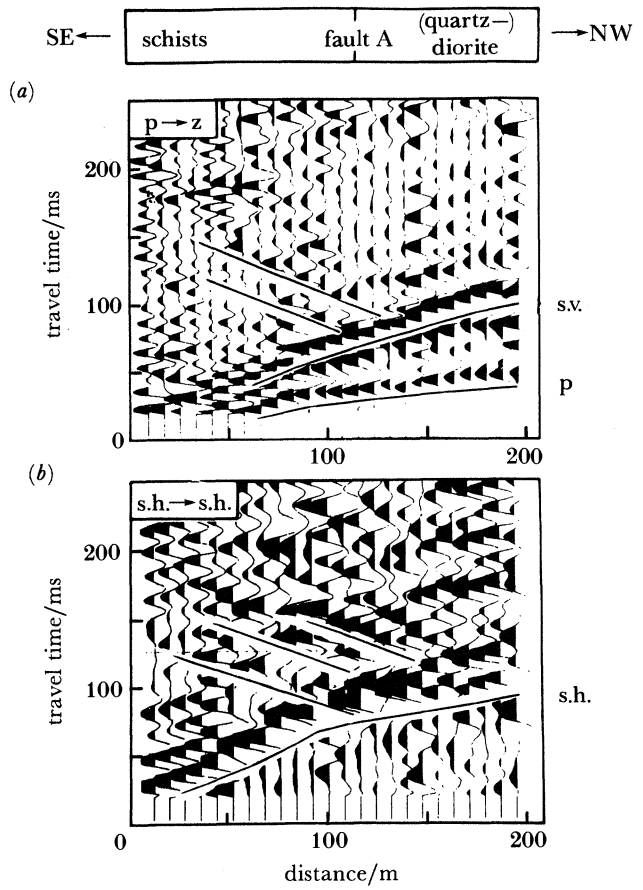

FIGURE 11. Refraction surveys across a fault zone (A): (*a*) compressional source and vertical receivers (p→z); first arrivals, p; second, s.v.; reflected at fault zone (A), s.v. (*b*) shear wave source and shear wave receivers (s.h.→s.h.); first arrivals, s.h.; reflected arrivals, s.h.

raypaths) was observed for the reversed arrangement along the shotpoints. A prism-shaped configuration of seismic rays had to be introduced to explain apparent velocities and travel times as shown in figure 12 (Meissner *et al.* 1980).

In addition to direct evidence for fault zones by the observations of reflections (figures 8, 10, 11, 12), some indirect signs like an offset of correlatable reflections or a pattern of diffractions along the fault may mark the trace of the fault. These indications are generally less reliable, especially diffraction patterns, which are very dense and nearly vertically arranged in the lower crust of the Moldanubian and Saxothuringian along the new DEKORP II S profile in the Variscides (in preparation). Such patterns are still highly debatable and provide serious problems for the interpreter.

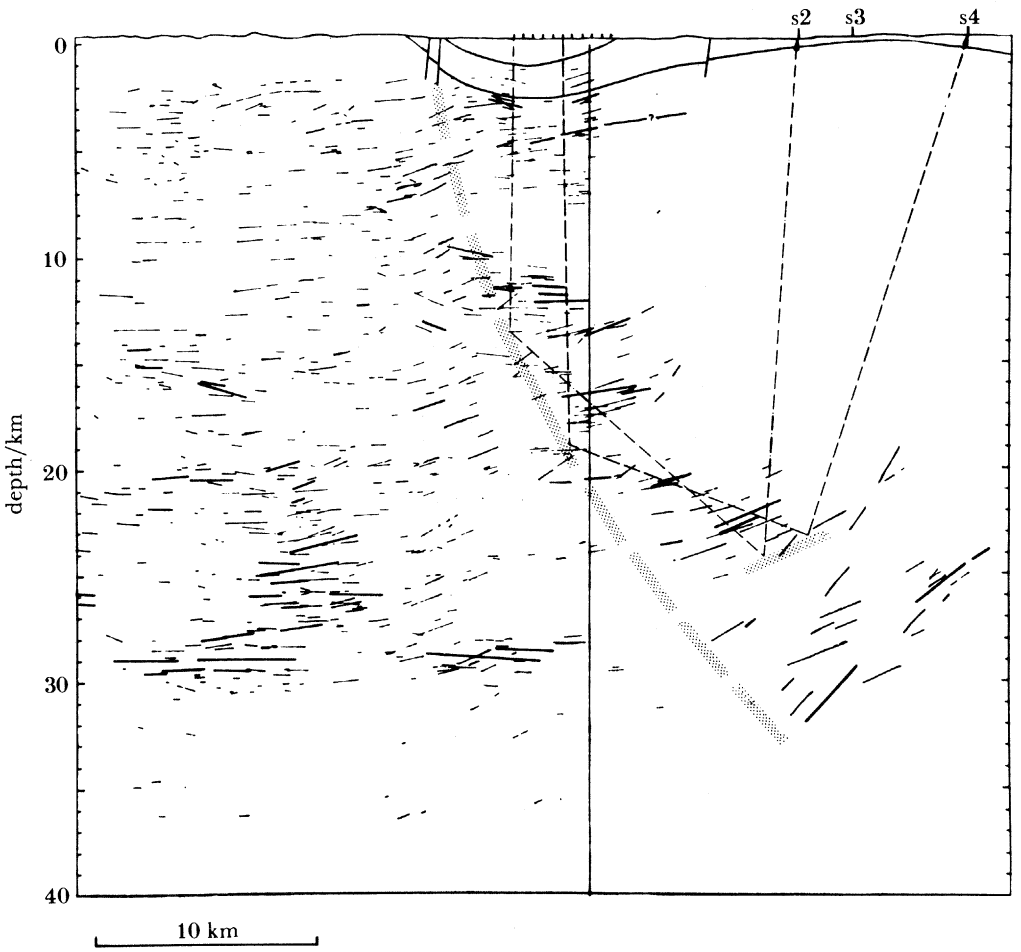

FIGURE 12. Seismic rays with nearly vertical ray paths (apparent velocities approaching one another), reflected at the fault zone and another dipping reflector near the Hunsrück boundary fault; see also figure 8*a*.

5. Discussion and conclusions

The restriction of seismicity to the upper continental crust and the similarity between the shape of the seismicity–depth curves and the theoretically and experimentally derived strength–depth or viscosity–depth curves are strong indications that the lower crust is a zone of high ductility, comparable with the jelly inside a two- or three-layered sandwich. It may

act as a buffer for any stress supposed to have its origin in the mantle. The mere appearance of mylonite structures in rocks from the lower crust, the subhorizontal detachment faults (see table 3) and the appearance of subhorizontal, reflecting lamellae in mature crusts (see figure 5*c*) provide additional evidence for the high ductility of the lower crust outside the old and rigid shield areas.

When calculating viscosity values for the oceanic lithosphere with its thin crust, it became apparent that the same viscosity values as calculated for the continental lower crust are found in the oceanic uppermost mantle at comparable depths of 20–30 km (Vetter & Meissner 1977, 1979). These observations may have important consequences with regard to zones of detachment and decoupling, which should be in a similar viscosity régime. Whereas during oceanic compression ophiolites, consisting of oceanic crust *and* part of the uppermost mantle (periodotites), form the thrusting sheets, compressional tectonics in continental environments produce nappes consisting of crustal rocks only. While oceanic plate tectonics deal with a simple 'single' plate, continental plate tectonics have to consider a 'sandwich' or 'double' plate. During continental collision only the upper part of the sandwich (the upper crust) is transferred to the top of another unit along zones of detachment.

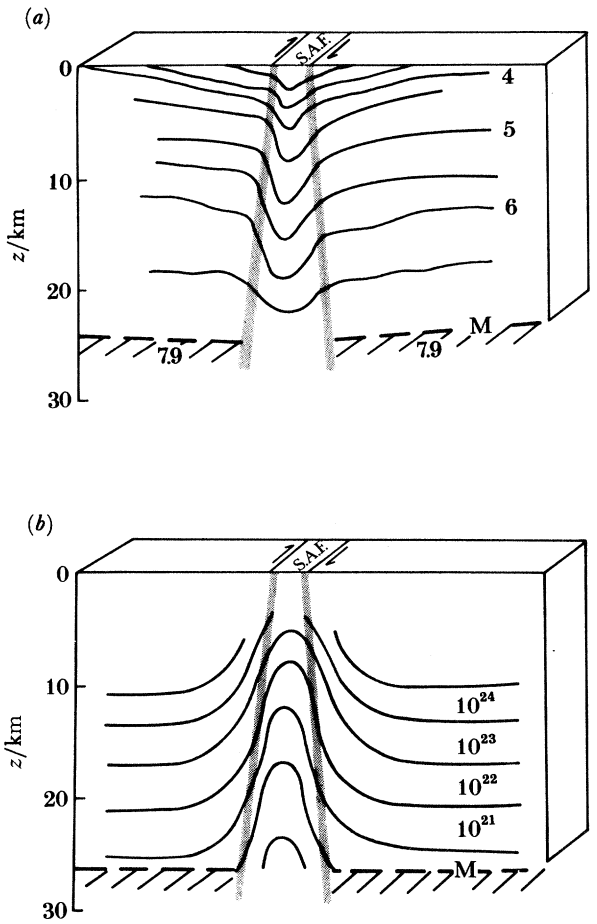

FIGURE 13. (*a*) Velocity structure near the San Andreas Fault (S.A.F.) (after Feng & McEvilly 1983); and (*b*) hypothetical viscosity structure, based on estimates of enhanced creep rate in the fault zone area. Velocity in kilometres per second, viscosity in poise. M is the Mohorovičić discontinuity.

A final question is related to the large strike-slip lineaments like the San Andreas or the North Anatolian Fault Zone. High strain rates might result in μ^* values lower than in 'ordinary' fault zones. As seen in table 3, μ^* values decrease to 0.4 and 0.35, but they do not reach the values for clay minerals (0.18). The lower μ^* values seem to agree with lower velocity values, showing a general weakening of the material. Figure 13*a* shows velocity isolines along the San Andreas Fault (Feng & McEvilly 1983). Also the stress and the viscosity values must be lower in accordance with the lower μ^* values. An estimate based on a concentration of creep in a 2 km wide zone of weakness results in the hypothetical viscosity structure of the San Andreas Fault Zone shown in figure 13*b*. Such lineaments are certainly pronounced anomalies of brittle and elastic, and also of inelastic, parameters.

References

Brace, W. F. 1972 Pore pressure in geophysics. In *Flow and fracture of rocks*, Geophysical Monograph vol. 16 (ed. H. C. Heard, I. Borg, N. L. Carter & G. B. Rayleigh), pp. 265–274. Washington: A.G.U.

Brace, W. F. 1979 Limits on crustal stress imposed by laboratory measurements. Paper presented at *Conference on Magnitude of Deviatoric Stress in the Earth's Crust and Upper Mantle*. U.S. Geological Survey, Carmel, California, 29 July to 2 August 1979.

Buffe, C., Harsh, P. & Burford, R. 1977 Steady-state seismic slip – a precise recurrence model. *Geophys. Res. Lett.* **4**, 91–94.

Byerlee, J. D. 1978 Friction of rocks. *Pure appl. Geophys.* **116**, 615–626.

Chen, W. P. & Molnar, P. 1983 Focal depths of intracontinental and intraplate earthquakes and their implications for the thermal and mechanical properties of the lithosphere. *J. geophys. Res.* **88**, 4183–4214.

Feng, R. & McEvilly, T. 1983 Interpretation of seismic reflection profiling data for the structure of the San Andreas Fault zone. *Bull. seism. Soc. Am.* **73**, 1701–1720.

Fountain, D. M., Hurich, C. A. & Smithson, S. B. 1984 Seismic reflectivity of mylonite zones in the crust. *Geology* **12**, 195–198.

Guterch, A. 1977 Structure and physical properties of the earth's crust in Poland in the light of new data of DSS. In *Polish Academy of Science, Proc. XV Gen. Ass. ESC*, pp. 347–357.

Illies, J. H. 1978 Two stages of Rhinegraben rifting. In *Tectonics and geophysics of continental rifts* (ed. I. B. Ramberg & E. R. Neumann), pp. 63–71. Dortrecht: Reidel.

Jaeger, J. C. 1969 *Elasticity, fracture and flow* (3rd edition), pp. 1–268. London: Methuen.

Jones, T. & Nur, A. 1982 Seismic velocity and anisotropy in mylonites and the reflectivity of deep crustal faults. *Geology* **10**, 260–263.

Jones, T. & Nur, A. 1984 The nature of seismic reflections from deep crustal fault zones. *J. geophys. Res.* **89**, 3153–3171.

Kirby, S. H. 1983 Rheology of the lithosphere. *Rev. Geophys. Space Phys.* **21**, 1458–1487.

Meissner, R. 1985 *The continental crust, a geophysical approach*. London: Academic Press. (In the press.)

Meissner, R., Bartelsen, H. & Murawski, H. 1980 Seismic reflection and refraction studies for investigating fault zones along the geotraverse Rhenoherzynikum. *Tectonophysics* **64**, 59–84.

Meissner, R., Bartelsen, H. & Murawski, H. 1981 Thin-skinned tectonics in the northern Renish Massif. *Nature, Lond.* **290**, 399–401.

Meissner, R. & Strehlau, J. 1982 Limits of stresses in the continental crust and their relation to depth–frequency distribution of shallow earthquakes. *Tectonics* **1**, 73–89.

Meissner, R. & Strehlau, J. 1985 Estimation of crustal viscosities and their role in geodynamic processes. In *The composition and dynamics of the lithosphere–asthenosphere system*. The International Lithosphere Program, working group 9. (In the press.)

Rabbel, W. 1985 Flachseismische Untersuchungen an Störungszonen. Dr-Thesis, Institut für Geophysik, Kiel University.

Sibson, R. H. 1974 Frictional constraints on thrust, wrench and normal faults, *Nature, Lond.* **249**, 542–545.

Sibson, R. H. 1977 Fault rocks and fault mechanisms. *J. geol. Soc. Lond.* **133**, 191–213.

Sibson, R. H. 1982 Fault zone models, heat flow and depth distribution of earthquakes in the continental crust of the United States. *Bull. seismol. Soc. Am.* **72**, 151–164.

Strehlau, J. 1985 *Erdbeben-Tiefen-Verteilung in verschiedenen Wärmestromgebieten. Dr-Thesis, Institut für Geophysik, Kiel University*.

Vetter, U. & Meissner, R. 1977 Creep in dynamic processes. *Tectonophysics* **42**, 37–54.

PHILOSOPHICAL TRANSACTIONS OF THE ROYAL SOCIETY A MATHEMATICAL, PHYSICAL & ENGINEERING SCIENCES

Vetter, U. & Meissner, R. 1979 Rheologic properties of the lithosphere and application to passive continental margins. *Tectonophysics* **59**, 369–380.

Wang, C. Y. 1984 On the constitution of the San Andreas Fault Zone in Central California. *J. geophys. Res.* **89**, 5858–5866.

Weertman, J. 1970 The creep strength of the earth's mantle. *Rev. Geophys. Space Phys.* **8**, 145–168.

Weertman, J. & Weertman, J. R. 1975 High-temperature creep of rock and mantle viscosity. *A. Rev. Earth planet. Sci.* **3**, 293–315.

Wise, D. U., Dunn, D., Engelder, J., Geiser, P., Hatcher, R., Kish, S., Odom, A. & Schamel, S. 1984 Fault-related rocks: suggestions for terminology. *Geology* **12**, 391–394.

Zoback, M. D. & Healy, J. H. 1984 Friction, faulting and *in situ* stress. *Anns Geophys.* **2**, 689–698.

Zoback, M. D. & Zoback, M. L. 1981 State of stress and intraplate earthquakes in the United States. *Science, Wash.* **213**, 96–104.

PHILOSOPHICAL TRANSACTIONS OF THE ROYAL SOCIETY A MATHEMATICAL, PHYSICAL & ENGINEERING SCIENCES